RSC Advances

ROYAL SOCIETY OF CHEMISTRY

www.rsc.org/advances

Cite this: DOI: 10.1039/c0xx00000x

www.rsc.org/xxxxxx

ARTICLE TYPE

Reducing Adhesion and Friction Forces of Si by Coating Ultra-thin Al_2O_3 Films

Zhimin Chai,[a] Yuhong Liu,[a] Xinchun Lu*[a] and Dannong He[b]

Received (in XXX, XXX) Xth XXXXXXXXX 20XX, Accepted Xth XXXXXXXXX 20XX

DOI: 10.1039/b000000x

Si-based microelectromechanical system (MEMS) devices cannot run reliably because of their poor tribological performance. Ultra-thin alumina (Al_2O_3) films are promising candidates to solve the tribological problems. In this study, adhesion and friction forces between a probe tip and ultra-thin alumina (Al_2O_3) films were studied by an atomic force microscope (AFM). The Al_2O_3 films with thickness of 0.8-5.0 nm were prepared on a Si (100) substrate by atomic layer deposition (ALD) using trimethyl aluminum (TMA) and water as precursors. The results show that both the adhesion and friction forces of the Al_2O_3 films are smaller than those of the Si (100) substrate. We attribute the low adhesion force of the Al_2O_3 films to their low surface energy and hydrophobic nature, and the low friction force of the Al_2O_3 films to their low adhesion force. We also calculated the adhesion force between an AFM tip and the samples. The theoretical adhesion force agrees well with the measured result.

1. Introduction

Nowadays, microelectromechanical system (MEMS) devices are commercially available in many applications, such as accelerometers used to trigger vehicle airbags, inkjet heads and micro-mirror displays.[1, 2] These commercial MEMS devices have either nonmoving parts or moving parts with a restricted lateral motion. Therefore, tribological problems, such as adhesion, friction and wear, can be avoided. However, in many other MEMS devices, such as micro gears and motors, moving, touching and rubbing parts are inevitable.[3, 4] Moreover, silicon (Si), commonly used to fabricate the MEMS devices, possesses a high friction and a low wear resistance, which makes these devices impracticable. If these tribological problems can be resolved, many exciting applications will be enabled. Various methods have been used for MEMS devices to reduce their friction and wear. One approach is to deposit self-assembled monolayers (SAMs) on the surface of MEMS devices.[5-9] The SAMs coatings can reduce the adhesion force of the Si material efficiently by reducing its surface energy and increasing its hydrophobicity. However, the SAMs coatings do not have enough wear resistance, which limits their practical application. An vapor phase lubrication (VPL) method can replenish the protective layer during contacting and sliding.[10-13] However, the main challenge is to package the MEMS devices to include the vapor feed system. Hard films, such as diamond-like carbon (DLC),[14, 15] tungsten (W),[16, 17] silicon carbide (SiC),[18, 19] titanium dioxide (TiO_2)[20, 21] and alumina (Al_2O_3)[22-24] can also reduce friction and wear of Si material, while how to coat the complicated structures of MEMS devices conformally is a matter of concern.

Many physical vapor deposition (PVD) technologies, such as sputtering deposition (SP), ion beam deposition (IBD) and pulsed laser deposition (PLD), are line-of-sight technologies, making them difficult to coat high aspect ratio and shadowed structures of MEMS devices uniformly.[25] Though chemical vapor deposition (CVD) technology has a high conformality, the temperature it requires during the reaction is quite high, which also limits its application in MEMS devices. Atomic layer deposition (ALD) is a branch of CVD, but the deposition temperature it requires can be much lower. ALD technology relies on a binary reaction in which two precursors are pulsed onto the substrate surface alternately, with a purge cycle between the two precursors.[26] The self-limiting character of ALD facilitates the growth of an ultra-thin and conformal film with an accurate thickness on a large area. This unique character makes the use of ALD in MEMS devices possible.

Al_2O_3 is a technologically important material due to its high mechanical strength and abrasive resistance.[27] These properties make Al_2O_3 films attractive in MEMS devices as protective coatings to reduce the adhesion, friction and wear.[25, 24, 28] With the continued shrinking of MEMS devices, the corresponding thickness of the Al_2O_3 films decreases. When the film thickness decreases to the sub-10nm scale, ALD is the best choice to grow such thin films with high thickness and constituent uniformity. However, even if ultra-thin films are conformally deposited on the MEMS devices, a question as to whether the ultra-thin films can provide tribological protection is still in doubt. The successful application of a ~4 nm DLC film in data storage devices has demonstrated that films in this thickness scale are capable to provide mechanical protection.[29] As a hard coating, Al_2O_3 film may be an alternate to the DLC film. The knowledge of a critical thickness at which Al_2O_3 film possesses superior tribological behavior to Si is important to ensure normal

operation of the MEMS devices.

In this study, Al_2O_3 films were grown by ALD on a Si (100) substrate at temperature of 200 °C. The adhesion and friction forces of the Al_2O_3 films were investigated by an atomic force microscope (AFM) in the ambient air. The resulting adhesion force is found to correlate with van der Waals force and capillary force. In addition, the friction force of the Al_2O_3 films correlates with their adhesion force. The adhesion and friction forces of the Al_2O_3 films are compared with those of the Si (100) substrate. The results in our study can provide much information for MEMS devices design.

2. Experimental methods

2.1 Film preparation

Al_2O_3 films were grown on a Si (100) substrate using a SUNALETM R-series ALD UNIT produced by Picosun. Trimethyl aluminum (TMA, purity >99.99%) was used as Al-precursor, and water (purity >99.99%) as O-precursor.[30, 31] The two precursors were delivered into a reaction chamber alternately with a high purity nitrogen (purity >99.999%) carrier flow, and between the two precursor cycles, the reaction chamber was purged with the high purity nitrogen. One completed ALD cycle consisted of 0.1 s of TMA/N_2, 3 s of N_2, 0.1 s of H_2O/N_2, and 4 s of N_2. Prior to film deposition, the Si (100) substrate was ultrasonically cleaned in acetone, absolute alcohol and deionized water for 10 min, respectively and then immersed into dilute hydrofluoric acid (HF) solution (HF: H_2O =1:100) for 30 s to remove the native oxide. During deposition, a dry pump was used to keep the base pressure of the reaction chamber ~600 Pa. 8-50 ALD cycles were completed at substrate temperature of 200 °C in order to obtain ultra-thin Al_2O_3 films with thickness below 10 nm.

2.2 Film characterization

The thickness of the Al_2O_3 films was measured by a null-ellipsometry (Multiskop, Optrel). The wavelength of the incident laser was 632.8 nm, and the incident angle was 70°. The resulting raw data were fitted by the Elli software (Optrel) using a three layer model (air/film/substrate).

To make clear whether the ultra-thin Al_2O_3 films were uniform and continuous, cross-sectional images of the films were obtained by a high resolution transmission electron microcopy (HRTEM, JEOL JEM 2010) operated at 200 kV. Samples for cross-sectional TEM observation were prepared by forming a sandwich structure with epoxy followed by mechanical polishing and then Ar ion milling. To distinguish the amorphous Al_2O_3 films from epoxy easily, a ~100 nm crystalline zinc oxide (ZnO) film was deposited by ALD on the Al_2O_3 films. The detailed process of ZnO film deposition can be seen in our previous study.[32]

The surface morphology of the Al_2O_3 films was measured by a NanoScope IIIA atomic force microscope (AFM, Veeco) in a tapping mode using a PPP-NCHR-20 probe (NanoSensors) with a spring constant of ~42 N/m and resonant frequency ~300 KHz. The root-mean-square (RMS) roughness value of the Al_2O_3 films was subsequently evaluated with the Nanoscope Software (Veeco).

The wettability of the Al_2O_3 films was investigated by a homemade static contact angle analyzer. We chose two kinds of liquids: water and ethylene glycol, which are polar and nonpolar liquids, respectively. A drop of liquid about 10 μL was dripped on the surface of the films by a microsyringe. The value of contact angle was determined by fitting the shape of the droplet using the instrument software. The mean value of contact angle was calculated from at least four individual readings and the typical measurement error was less than 2°.

2.3 Adhesion and friction forces

The adhesion force of the Al_2O_3 films was measured by the AFM (Veeco) in a force calibration mode[33] using a commercial NP-10 probe (Bruker). The probe tip is made of Si_3N_4. The Si_3N_4 tip has a large hardness and thus cannot be worn easily. In addition, Si_3N_4 has similar mechanical properties to Al_2O_3. Therefore, Si_3N_4 was used to replace Al_2O_3 to model Al_2O_3 against Al_2O_3 in MEMS devices. The normal spring constant of the AFM probe calibrated using the thermal noise method was 0.61 N/m, and the radius of the AFM tip measured by a TGT01 (NT-MDT) grating was ~50 nm (as detailed in the Supplementary Information). All experiments were made at a temperature of 26 ± 0.5 °C and a relative humidity of 55 ± 5%. Firstly, a 4 × 4 μm^2 topography image of the Al_2O_3 films was acquired in a contact mode. Once the scanner stopped, force–distance curves were obtained at 16 different locations. The adhesion force was measured directly from the force curves.

The friction force of the Al_2O_3 films was measured by the AFM (Veeco) in a contact mode using the same probe as that in the adhesion experiment. In addition, the experimental temperature and relative humidity are the same to those of the adhesion experiment. The AFM tip scanned on the Al_2O_3 films in a direction orthogonal to the cantilever, resulting in a torsion, which corresponded to the friction force between the AFM tip and the Al_2O_3 films. The scanning area was 1 × 0.1 μm^2, and the scan speed was 3 μm/s. The normal load exerted on the Al_2O_3 films was controlled by adjusting the deflection of the cantilever. Because the raw friction force was in the unit of volt (V), calibration of the AFM probe should be conducted to convert the unit to Newton (N). The wedge calibration method was used in our experiment,[35, 36] and the calibration specimen was a TGF11 grating (Mikromasch) with a slope angle of 54.73°.

3. Results and discussion

3.1 Film properties

To get ultra-thin Al_2O_3 films, controlling the growth rate precisely becomes the critical issue. In theory, the ALD technique can ensure the precise thickness control at the angstrom (Å) or monolayer level.[37] Therefore, the ultra-thin Al_2O_3 films in our study was prepared by ALD. The film thickness was controlled by adjusting the number of ALD cycles. Figure 1 shows the Al_2O_3 film thickness as a function of ALD cycles. Each value in the figure is an average of 6 points measured by the ellipsometer at different locations of the films. The film thicknesses increase linearly with the number of ALD cycles. The dash line is least squares fit of the thickness value, whose slope gives a growth rate of 0.098 nm/cycle, which agrees well with previously reported 0.09 nm/cycle.[38, 39]

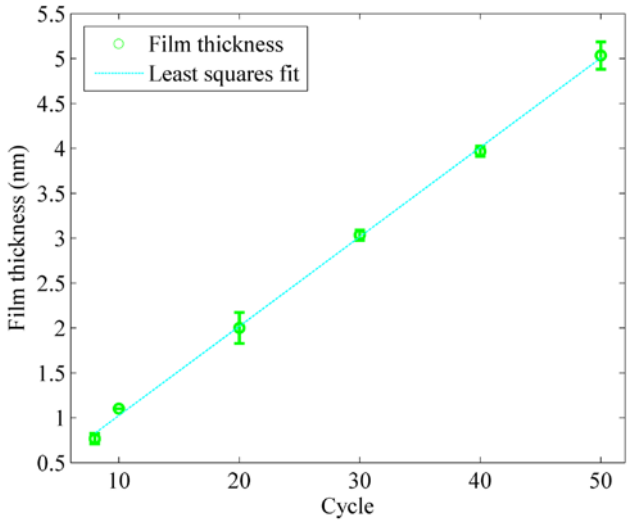

Figure 1. Al_2O_3 film thicknesses as a function of the number of ALD cycles.

High resolution cross-sectional TEM image was used to observe the continuity of the Al_2O_3 films. Figure 2 (a) and (b) show the TEM images of the Al_2O_3 films deposited at 8 and 20 ALD cycles, respectively. The crystalline regions in the images are the Si (100) substrate and the ZnO film. Between the crystalline regions, thin Al_2O_3 films can be found. It should be noted that the Al_2O_3 films are primarily amorphous. In Figure 2 (a), no obvious SiO_2 native oxide layer is visible because the Si (100) substrate was treated by the HF solution. The film thickness is measured to be 1.0 nm, which is slightly larger than that obtained by the ellipsometer. The difference in film thickness may result from tilt of TEM sample. The 1.0 nm Al_2O_3 film is not dense and continuous, as shown in Figure 2 (a). When the number of ALD cycles increases to 20, the thickness of Al_2O_3 film reaches 2.0 nm, and the film becomes dense and continuous, as shown in Figure 2 (b). For the 2.0 nm Al_2O_3 film, the Si (100) substrate was not pretreated by the HF solution, and thus an interfacial layer of 1.2 nm is visible between the Al_2O_3 film and the Si (100) substrate.

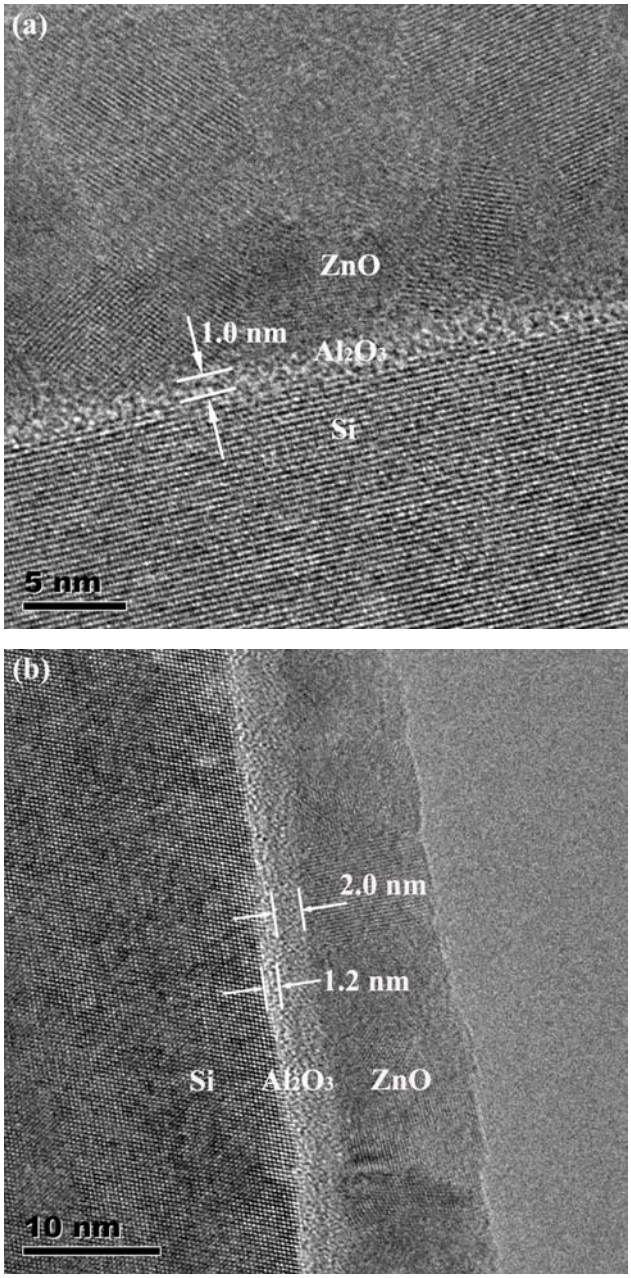

Figure 2. High resolution cross-sectional TEM images of the Al_2O_3 films deposited at 8 (a) and 20 (b) ALD cycles, respectively.

Figure 3 shows the RMS roughness of the Al_2O_3 films with various film thicknesses, and the inset is the three-dimensional (3D) AFM image of the 2.0 nm thick Al_2O_3 film. It can be seen that the RMS roughness of the Al_2O_3 films changes little with the increase of film thickness. The RMS roughness values are ~0.5 nm, which is slightly larger than 0.35 nm of the Si (100) substrate. Because the surfaces of the Al_2O_3 films are atomically smooth, the influence of surface roughness on adhesion[40-43] and friction can be ignored.

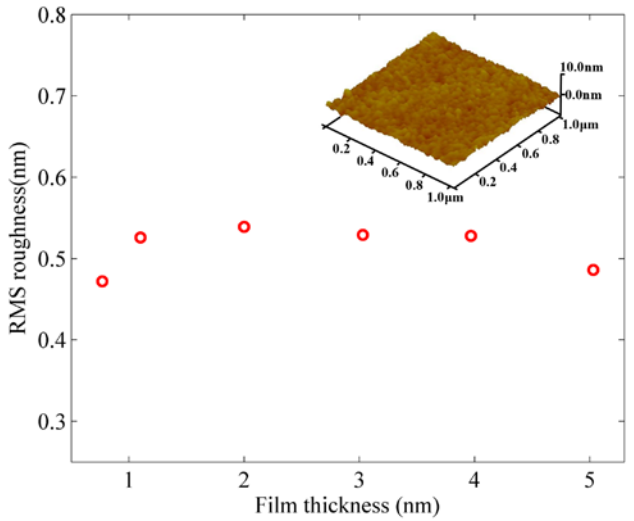

Figure 3. The RMS roughness of the Al_2O_3 films as a function of film thickness; the inset is the 3D AFM image of the 2.0 nm thick Al_2O_3 film.

The wetting ability of the Al_2O_3 films was studied by the static contact angle measurement. Figure 4 (a) shows the contact angles of water on the Al_2O_3 films with various thicknesses. The contact angle of the Al_2O_3 films is about 100° and almost constant for various thicknesses, which is much larger than 50.3 ± 0.6° of the Si (100) substrate and 23.0 ± 0.5° of the Si_3N_4 tip.[44] Because the contact angle of the Al_2O_3 films is larger than 90°, the surfaces of films are hydrophobic. The hydrophobic property of the Al_2O_3 films may be attributed to the residual TMA precursor in the Al_2O_3 films.[45] Due to the hydrophobic nature of the Al_2O_3 films, the capillary force component of the adhesion force can be significantly reduced, which will be discussed below.

The contact angles of ethylene glycol on the Al_2O_3 films are also shown in Figure 4 (a), with values of about 75°. From the contact angles of the two liquids, the polar (γ_S^p) and nonpolar (γ_S^d) components and the total surface energy (γ_S) of the Al_2O_3 films can be calculated according to the Owens and Wendt approach:[46]

$$\gamma_S = \gamma_S^d + \gamma_S^p \quad (1)$$

$$\gamma_L = \gamma_L^d + \gamma_L^p \quad (2)$$

$$\gamma_L(1+\cos\theta) = 2\left(\sqrt{\gamma_S^d \gamma_L^d} + \sqrt{\gamma_S^p \gamma_L^p}\right) \quad (3)$$

where γ_L is the surface tension of liquids, γ_L^d and γ_L^p refer the non-polar and polar components of the surface tension of liquids, and θ is the contact angle of liquids. The surface tensions of water and ethylene glycol are listed in the Table 1, and the calculated surface energy and its components of the Al_2O_3 films are shown in Figure 4 (b). It can be seen that the surface energies of the Al_2O_3 films are in the range of 21.6-24.6 mJ/m^2, which are smaller than 44.8 mJ/m^2 of the Si (100) substrate (Table 1) and 48.3 mJ/m^2 of the Si_3N_4 tip (Table 1).[44] The variation in surface energy can be assigned to small differences in the contact angle.

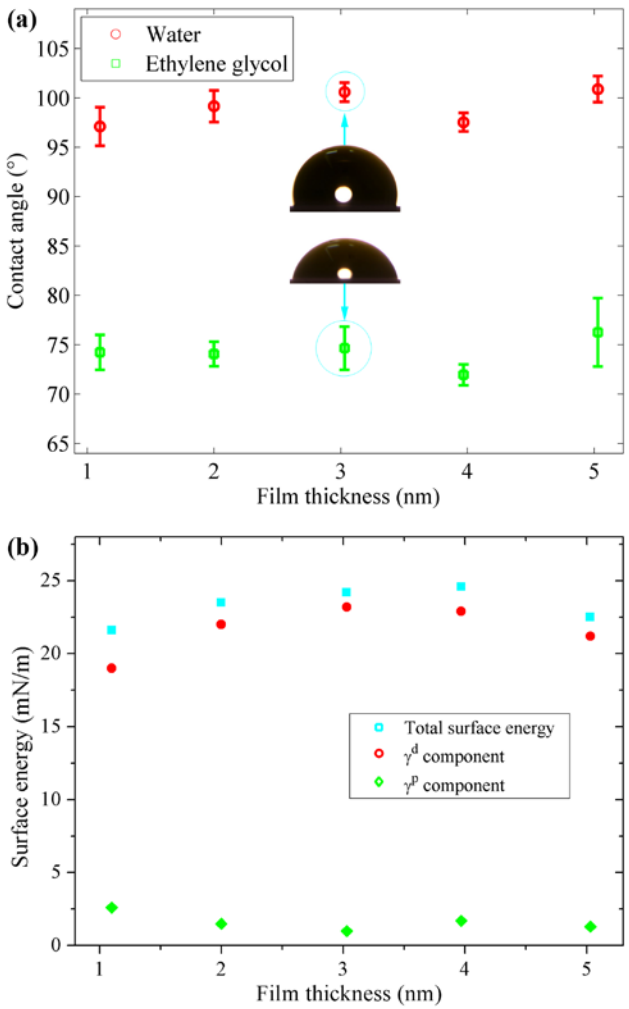

Figure 4. (a) The contact angles of water and ethylene glycol on the Al_2O_3 films with various thicknesses. The upper and lower insets show water droplet and ethylene glycol droplet on the 3.0 nm thick Al_2O_3 film, respectively. (b) The surface energy and its components of the Al_2O_3 films as a function of film thickness.

Table 1. Surface energy and its components for the liquids used in contact angle experiment, the Si (100) substrate and the Si_3N_4 tip

	γ^d (mN/m)	γ^p (mN/m)	γ_{total} (mN/m)
Water	21.8	51.0	72.8
Ethylene glycol	29.0	19.0	48.0
Si (100)[a]	36.5	8.3	44.8
Si_3N_4 (tip)[a]	38.0	10.3	48.3

[a]From ref [44]. The polar (γ^p) component was calculated by $\gamma^p = 2\sqrt{\gamma^+\gamma^-}$

3.2 Adhesion force

When two surfaces come into contact, adhesion between them occurs. At the nanoscale, the adhesion force can be equivalent to the actuation force, and thus should be especially concerned. The adhesion force was measured by the AFM with the NP-10 probe. Figure 5 (a) shows the adhesion forces between the AFM tip and the Al_2O_3 films with various thicknesses. For comparison, the adhesion force of the Si (100) substrate is plotted in Figure 5 (b). It can be seen that the adhesion force of the Al_2O_3 films varies

slightly with film thickness. The variation of the adhesion force can be attributed to various factors, such as the variation of nanoscale surface roughness,[40] surface energy and contact angle. Moreover, the adhesion forces of the Al_2O_3 films are much lower than that of the Si (100) substrate. This means that the Al_2O_3 films can be used as protective coatings to reduce the adhesion force of Si material.

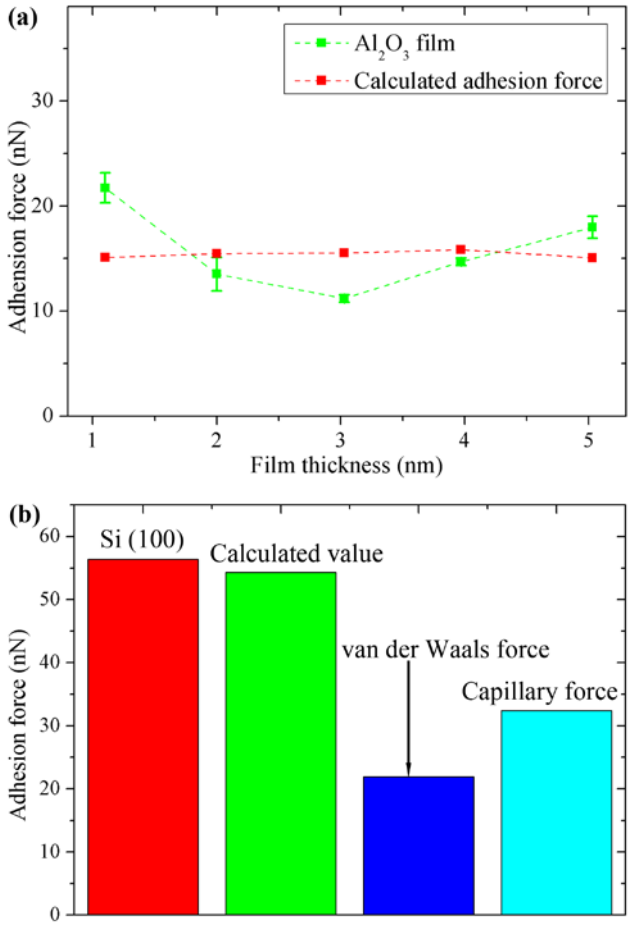

Figure 5. (a) The adhesion forces between the NP-10 probe and the Al_2O_3 films with various thicknesses. The green dashed line is the experimental result, and the red dashed line is the calculated result. (b) The experimental (red bar) adhesion force of the Si (100) substrate. The other three bars denote the calculated (green bar) adhesion force and its van der Waals component (blue bar) and capillary component (cyan bar).

As mentioned above, the surfaces of the Al_2O_3 films are atomically smooth. For the contact between a spherical tip and a smooth surface in the humidity environment, as shown in Figure 6, the adhesion force is given by

$$F_a = \frac{3}{2}\pi R_{tip} W_{12} + 2\pi R_{tip}\gamma_W \left(2c - \frac{D}{r_k}\right) \quad (4)$$

with

$$c = \frac{\cos\theta_1 + \cos\theta_2}{2} \quad (5)$$

where R_{tip} is the radius of the sphere, W_{12} is the work of adhesion per unit contact area, γ_W is the surface tension of the water, θ_1 is the contact angle of water on the sample surface, θ_2 is the contact angle of water on the tip surface, D (approximately 0.3 nm) is the minimum separation between the tip and the sample, and r_k is the equilibrium radius of the meniscus. The first term in Equation (4) is a contribution from the van der Waals force, and the second term is a contribution from the capillary force. It should be noted that a water film can hardly condense on a hydrophobic surface.[47-49] Accordingly, the capillary force can be neglected for the hydrophobic Al_2O_3 films.

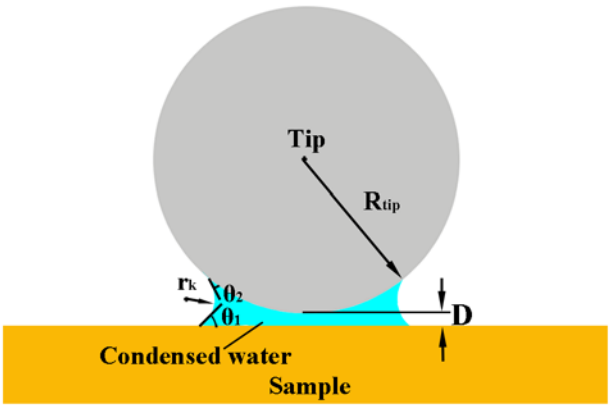

Figure 6. Schematic illustration of a spherical AFM tip contacting with a smooth surface.

The work of adhesion between two solids is related to their surface energy values by the following equation:[50]

$$W_{12} = 2\left[\left(\gamma_1^d \gamma_2^d\right)^{1/2} + \left(\gamma_1^p \gamma_2^p\right)^{1/2}\right] \quad (6)$$

Using the surface energy presented in Figure 4 (b) and Table 1, the work of adhesion between the Al_2O_3 films and the AFM tip is calculated, as shown in Figure 7.

The equilibrium radius of the meniscus is calculated by:[51, 52]

$$r_k = -\frac{\gamma_W V_m}{RT\ln(P/P_0)} \quad (7)$$

where V_m is the molar volume of water, R is the molar gas constant, T is the temperature, P is the vapor pressure, and P_0 is the saturated vapor pressure. It should be noted that P/P_0 is the relative humidity (RH). For T=300 K and RH=55%, the equilibrium radius r_k=2.1 nm.

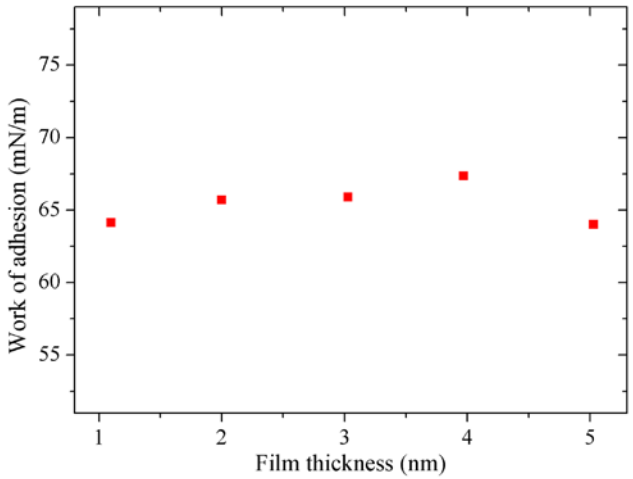

Figure 7. Work of adhesion between the Al_2O_3 films and the AFM tip.

The red dashed line presented in Figure 5 (a) is the adhesion force of the Al_2O_3 films calculated using Equation (4). Because of the hydrophobic nature of the Al_2O_3 films, the capillary force component is neglected, and only the van der Waals force component contributes to the adhesion force. The calculated adhesion force agrees well with the experimental results. From Figure 7, we can see that the work of adhesion between the Al_2O_3 films and the AFM tip does not vary greatly with film thickness. Therefore, the adhesion force does not vary greatly with film thickness.

It should be mentioned that the adhesion force in Figure 5 (a) is between the Si_3N_4 tip and the Al_2O_3 films. In order to model the real condition in MEMS devices, the adhesion between Al_2O_3 film and Al_2O_3 film should be measured. Because Al_2O_3 film and Si_3N_4 have different surface chemical properties, such as contact angle and surface energy, the adhesion force between Si_3N_4 tip and Al_2O_3 film differs with that between Al_2O_3 and Al_2O_3 film. Due to the hydrophilic nature and the large surface energy of Si_3N_4, the adhesion force between Si_3N_4 tip and Al_2O_3 film is larger than that between Al_2O_3 and Al_2O_3 film. However, as mentioned above, the adhesion force can be calculated by the equations in this paper, and the calculated adhesion force is consistent well with the measured value. Therefore, to get the adhesion force between Al_2O_3 and Al_2O_3 film, we just need to replace the parameter of Si_3N_4 with that of Al_2O_3.

The green bar in Figure 5 (b) is calculated adhesion force between the Si (100) substrate and the AFM tip. The calculated adhesion force also agrees well with the experimental results. For the hydrophilic Si (100) substrate, the capillary force cannot be neglected, and not only that, the value of capillary force is 32.4 nN, larger than 21.9 nN of van der Waals force. Because of the large surface energy of the Si (100) substrate, the van der Waals force between the AFM tip and the Si (100) substrate is larger than that between the Al_2O_3 films, which is ~15 nN. Because both the van der Waals and capillary force components of the Si (100) substrate is larger than that of the Al_2O_3 films, the total adhesion force of the Si (100) substrate is larger correspondingly.

3.3 Friction force

After the adhesion experiment, the friction experiment was made by the AFM using the same probe. By adjusting the deflection of cantilever, the normal loads in the range of 66-203 nN were exerted on samples. Figure 8 (a) shows the friction force of the Al_2O_3 films as a function of normal load, and Figure 8 (b) is the friction force of the Si (100) substrate. It can be seen that the friction force increases with normal load for all the samples and that for a fixed normal load the friction force seems to vary with similar trend to the adhesion force: the 3.0 nm thick Al_2O_3 film possesses the smallest adhesion force and the smallest friction force, while the 1.1 and 5.0 nm thick Al_2O_3 films possesses large adhesion force and large friction force. This means that the friction force of the Al_2O_3 films is dominated by the adhesion force.

The friction force of the Si (100) substrate is also dominated by the adhesion force. Because the Si (100) substrate possesses a much larger adhesion force than that of the Al_2O_3 films, the friction force of the Si (100) substrate is larger than that of the Al_2O_3 films correspondingly. The small friction force of the Al_2O_3 films makes it possible to reduce friction force of Si-based MEMS devices.

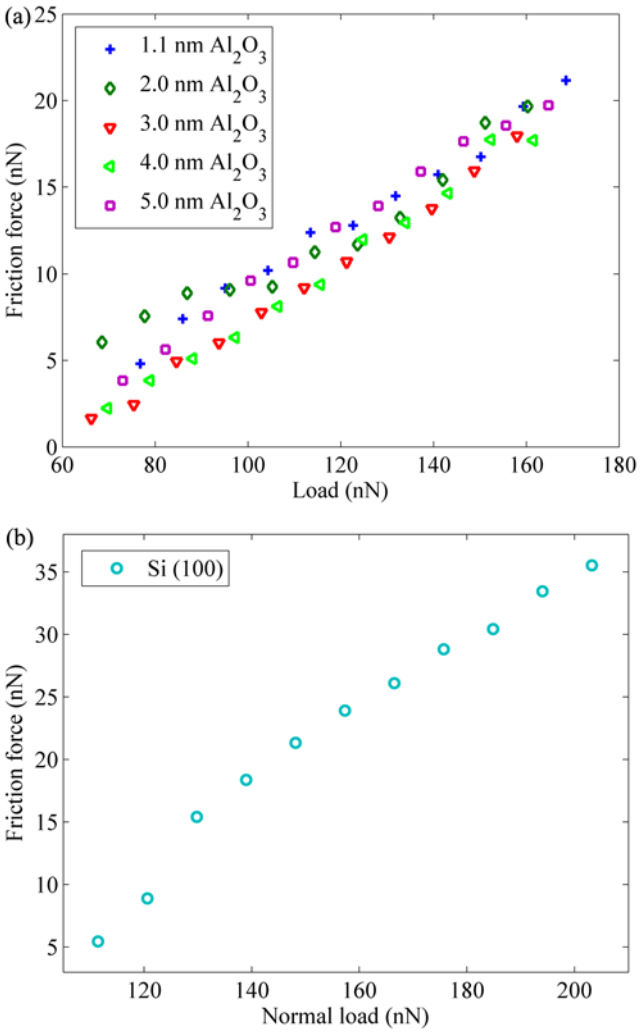

Figure 8. (a) The friction force of the Al_2O_3 films as a function of normal load. (b) The friction force of the Si (100) substrate as a function of normal load.

Conclusions

We have measured adhesion and friction forces between an AFM tip and ultra-thin Al_2O_3 films (with thickness in the range of 1.1-5.0 nm) prepared by atomic layer deposition. The adhesion measurement shows that the adhesion force of the Al_2O_3 films varies slightly with film thickness. The slight variation of the adhesion force is likely to be attributed to the variation of nanoscale surface roughness, surface energy and contact angle. Moreover, the adhesion forces of the Al_2O_3 films are much lower than that of the Si (100) substrate due to their hydrophobic nature. The measured adhesion force agrees well with the theoretical result. For the hydrophobic Al_2O_3 films, the capillary force component of the adhesion force can be neglected, and only the van der Waals force component contributes to the adhesion force, while for the Si (100) substrate, both the van der Waals and capillary force components contribute to the adhesion force.

The friction force between the AFM tip and the Al_2O_3 films was studied as a function of normal load. For a fixed normal load, the friction force varies with similar trend to the adhesion force, which demonstrates that friction force is dominated by the adhesion force. The friction force of the Al_2O_3 films is smaller than that of the Si (100) substrate due to the smaller adhesion force.

Our studies demonstrate that Al_2O_3 films with thickness in the sub-5 nm scale can effectively reduce the adhesion and friction forces of the Si (100) substrate, which indicates that the ultra-thin Al_2O_3 films are capable of being used as protecting coatings in Si-based MEMS devices to solve their tribological problems.

Acknowledgment

The authors greatly appreciate the financial support of the National Science Fund for Distinguished Young Scholars (50825501), the Science Fund for Creative Research Groups (51321092), the National Natural Science Foundation of China (51335005), and the National Science and Technology Major Project (2008ZX02104-001). Helpful discussions with Wen Jing are gratefully acknowledged.

Notes and references

[a] *The State Key Laboratory of Tribology, Tsinghua University, Beijing 100084, China.*
[b] *National Engineering Research Center for Nano technology, Shanghai 200241, China*
** Telephone/Fax: +86 10 6279 7362; E-mail addresses: xclu@tsinghua.edu.cn*

† Electronic Supplementary Information (ESI) available: AFM image of the NP-10 probe (Figure 1S). See DOI: 10.1039/b000000x/

1 S. H. Kim, D. B. Asay and M. T. Dugger, *Nano Today*, 2007, **2**, 22.
2 J. A. Williams and H. R. Le, *J. Phys. D: Appl. Phys.*, 2006, **39**, R201.
3 D. Berman and J. Krim, *Prog. Surf. Sci.*, 2013, **88**, 171.
4 M. T. Dugger, *Proc. SPIE* 2011, **8031**, 80311H.
5 H. Xiang and K. Komvopoulos, *J. Appl. Phys.*, 2013, **113**, 224505.
6 I. Laboriante, M. Fisch, A. Payamipour, F. Liu, C. Carraro and R. Maboudian, *Tribol. Lett.*, 2011, **44**, 13.
7 D. A. Hook, S. J. Timpe, M. T. Dugger and J. Krim, *J. Appl. Phys.*, 2008, **104**, 034303.
8 Y. H. Liu, P. X. Liu, Y. Q. Xiao and J. B. Luo, *Appl. Surf. Sci.*, 2012, **258**, 8533.
9 Y. H. Liu, X. K. Wang, J. B. Luo and X. C. Lu, *Appl. Surf. Sci.*, 2009, **255**, 9430.
10 A. L. Barnette, D. B. Asay, J. A. Ohlhausen, M. T. Dugger and S. H. Kim, *Langmuir*, 2010, **26**, 16299.
11 D. B. Asay, M. T. Dugger, J. A. Ohlhausen and S. H. Kim, *Langmuir*, 2008, **24**, 155.
12 D. B. Asay, M. T. Dugger and S. H. Kim, *Tribol. Lett.*, 2008, **29**, 67.
13 K. Strawhecker, D. B. Asay, J. McKinney and S. H. Kim, *Tribol. Lett.*, 2005, **19**, 17.
14 L. Xin, Z. Chao and L. Jun, *Proc. of SPIE*, 2009, **7133**, 713347.
15 S. A. Smallwood, K. C. Eapen, S. T. Patton and J. S. Zabinski, *Wear*, 2006, **260**, 1179.
16 S. S. Mani, J. G. Fleming, J. A. Walraven, J. J. Sniegowski, M. P. Se Beer, L. W. Irwin, D. M. Tanner, D. A. LaVan, M. T. Dugger, J. Jakubczak and W. M. Miller, 2000 IEEE International Reliability Physics Symposium Proceedings, California, 2000.
17 J. A. Walraven, S. S. Mani, J. G. Fleming, T. J. Headley, P. G. Kotula, A. A. Pimentel, M. J. Rye, D. M. Tanner and N. F. Smith, Proc. SPIE, 2000, 4180, 49.
18 F. Xiao-An, J. L. Dunning, M. Mehregany and C. A. Zorman, *J. Electrochem. Soc.*, 2011, **158**, 675.
19 R. Anzalone, G. D'Arrigo, M. Camarda, C. Locke, S. E. Saddow and F. La Via, *J. Microelectromech. Syst.*, 2011, **20**, 745.
20 C. Nistorica, J. F. Liu, I. Gory, G. D. Skidmore, F. M. Mantiziba, B. E. Gnade and J. Kim, *J. Vac. Sci. Technol. A*, 2005, **23**, 836.
21 Y. J. Huang, G. Pandraud and P. M. Sarro, *J. Vac. Sci. Technol. A*, 2013, **31**, 01A148.
22 C. Nistorica, I. Gory and G. D. Skidmore, *Mater. Res. Soc. Symp. Proc.*, 2005, **841**, R9.16.
23 N. Hoivik, J. Elam, R. Linderman, V. M. Bright, S. George and Y. C. Lee, Fifteenth IEEE International Conference on Micro Electro Mechanical Systems, NEW YORK, 2002.
24 N. D. Hoivik, J. W. Elam, R. J. Linderman, V. M. Bright, S. M. George and Y. C. Lee, *Sensor. Actuat. A*, 2003, **103**, 100.
25 T. M. Mayer, J. W. Elam, S. M. George, P. G. Kotula and R. S. Goeke, *Appl. Phys. Lett.*, 2003, **82**, 2883.
26 M. Leskela and M. Ritala, *Thin Solid Films*, 2002, **409**, 138.
27 M. D. Groner, J. W. Elam, F. H. Fabreguette and S. M. George, *Thin Solid Films*, 2002, **413**, 186.
28 A. Aryasomayajula, N. X. Randall, M. H. Gordon and D. Bhat, *Thin Solid Films*, 2008, **517**, 819.
29 C. Casiraghi, J. Robertson and A. C. Ferrari, *Materials Today*, 2007, **10**, 44.
30 A. W. Ott, K. C. McCarley, J. W. Klaus, J. D. Way and S. M. George, *Appl. Surf. Sci.*, 1996, **107**, 128.
31 M. Juppo, A. Rahtu, M. Ritala and M. Leskela, *Langmuir*, 2000, **16**, 4034.
32 Z. M. Chai, X. C. Lu and D. N. He, *Surf. Coat. Tech.*, 2012, **207**, 361.
33 B. Bhushan and S. Sundararajan, *Acta Mater.*, 1998, **46**, 3793.
34 H. J. Butt and M. Jaschke, *Nanotechnology*, 1995, **6**, 1.
35 D. F. Ogletree, R. W. Carpick and M. Salmeron, *Rev. Sci. Instrum.*, 1996, **67**, 3298.
36 M. Varenberg, I. Etsion and G. Halperin, *Rev. Sci. Instrum.*, 2003, **74**, 3362.
37 S. M. George, *Chem. Rev.*, 2010, **110**, 111.
38 A. W. Ott, J. W. Klaus, J. M. Johnson and S. M. George, *Thin Solid Films*, 1997, **292**, 135.
39 R. Matero, A. Rahtu, M. Ritala, M. Leskela and T. Sajavaara, *Thin Solid Films*, 2000, **368**, 1.
40 Z. Chai, Y. Liu, X. Lu and D. He, *ACS Appl. Mater. Interfaces*, 2014.
41 S. N. Ramakrishna, L. Y. Clasohm, A. Rao and N. D. Spencer, *Langmuir*, 2011, **27**, 9972.
42 Y. I. Rabinovich, J. J. Adler, M. S. Esayanur, A. Ata, R. K. Singh and B. M. Moudgil, *Adv. Colloid Interface Sci.*, 2002, **96**, 213.
43 J. Katainen, M. Paajanen, E. Ahtola, V. Pore and J. Lahtinen, *J. Colloid Interface Sci.*, 2006, **304**, 524.
44 C. Jacquot and J. Takadoum, *J. Adhes. Sci. Technol.*, 2001, **15**, 681.
45 Z. Chai, Y. Liu, X. Lu and D. He, *Tribol. Lett.*, 2014, **55**, 143.
46 D. K. Owens and R. C. Wendt, *J. Appl. Polym. Sci.*, 1969, **13**, 1741.
47 B. Bhushan, Nanomechanics, and Materials Characterization. In *Nanotribology and Nanomechanics II*, 3rd ed. B. Bushan, Springer, Heidelberg, Germany, 2004, pp 3-106.

48 Y. C. Liao, W. Hargrove and B. L. Weeks, *Sci. World J.*, 2013, **748295**, 1.
49 S. Darwich, K. Mougin, A. Rao, E. Gnecco, S. Jayaraman and H. Haidara, *Beilstein J. Nanotechnol.*, 2011, **2**, 85.
50 J. N. Israelachvili, In *Intermoiecuilar and surface forces*, 3rd ed. Academic Press, Burlington, 2011, pp 415-419**.**
51 H. J. Butt and M. Kappl, *Adv. Colloid Interface Sci.*, 2009, **146**, 48..
52 P. J. van Zwol, G. Palasantzas and J. De Hosson, *Phys. Rev. E*, 2008, **78**, 031606.

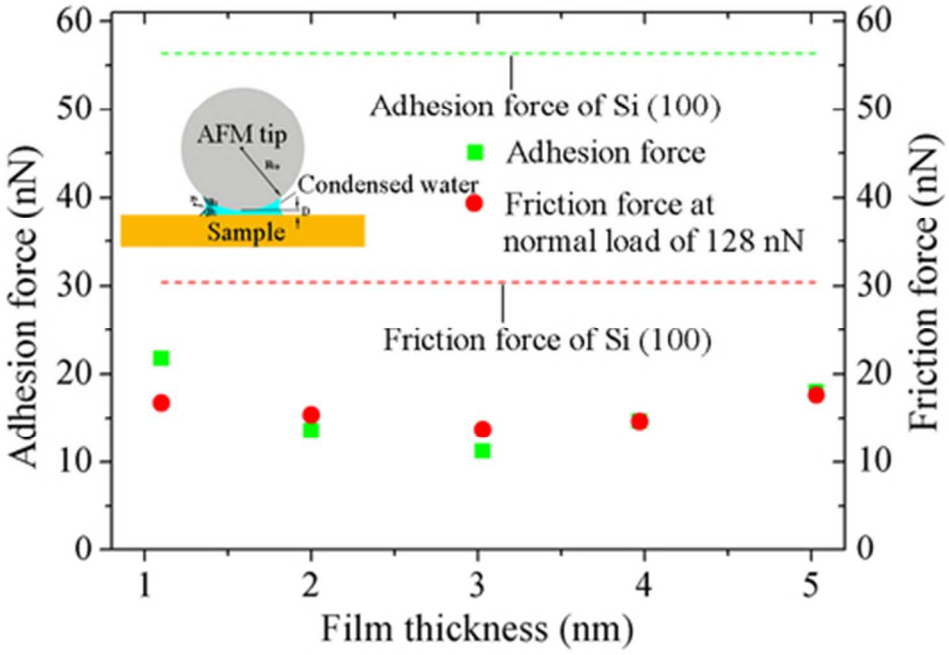

39x27mm (300 x 300 DPI)